Published in final edited form as:
Vis Neurosci. 2009 ; 26(3): 287–296. doi:10.1017/S0952523809090075.

Parvalbumin-immunoreactive amacrine cells of macaque retina

Kathryn E. Klump[1], **Ai-Jun Zhang**[2], **Samuel M. Wu**[2], and **David W. Marshak**[1]

[1]Department of Neurobiology and Anatomy, University of Texas Medical School at Houston, Houston, Texas

[2]Cullen Eye Institute, Baylor College of Medicine, Houston, Texas

Abstract

A number of authors have observed amacrine cells containing high levels of immunoreactive parvalbumin in primate retinas. The experiments described here were designed to identify these cells morphologically, to determine their neurotransmitter, to record their light responses, and to describe the other cells that they contact. Macaque retinas were fixed in paraformaldehyde and labeled with antibodies to parvalbumin and one or two other markers, and this double- and triple-labeled material was analyzed by confocal microscopy. In their morphology and dendritic stratification patterns, the parvalbumin-positive cells closely resembled the knotty type 2 amacrine cells described using the Golgi method in macaques. They contained immunoreactive glycine transporter, but not immunoreactive γ-aminobutyric acid, and therefore, they use glycine as their neurotransmitter. Their spatial density was relatively high, roughly half that of AII amacrine cells. They contacted lobular dendrites of AII cells, and they are expected to be presynaptic to AII cells based on earlier ultrastructural studies. They also made extensive contacts with axon terminals of OFF midget bipolar cells whose polarity cannot be predicted with certainty. A macaque amacrine cell of the same morphological type depolarized at the onset of increments in light intensity, and it was well coupled to other amacrine cells. Previously, we described amacrine cells like these that contacted OFF parasol ganglion cells and OFF starburst amacrine cells. Taken together, these findings suggest that one function of these amacrine cells is to inhibit the transmission of signals from rods to OFF bipolar cells *via* AII amacrine cells. Another function may be inhibition of the OFF pathway following increments in light intensity.

Keywords

Monkey; Bipolar; Glycine; Midget; Parasol

Introduction

Amacrine cells are local circuit neurons that ramify in the inner plexiform layer (IPL) of the retina, where they make synapses onto axon terminals of bipolar cells, dendrites of retinal ganglion cells, and dendrites of other amacrine cells (Dowling & Boycott, 1966). Anatomical studies suggest that amacrine cells play a major role in the processing of visual information in the IPL. In primates, synapses made by amacrine cells are, by far, the most common type there; they outnumber synapses made by bipolar cells by a factor of 3 in the central retina and a factor of 4 in the peripheral retina. Of the various kinds of amacrine cell synapses, those onto other amacrine cells are the most common (Koontz & Hendrickson,

Address correspondence and reprint requests to: David W. Marshak, Department of Neurobiology and Anatomy, University of Texas Medical School at Houston, PO Box 20708, Houston, TX 77225. david.w.marshak@uth.tmc.edu.

1987). Primate amacrine cells have been subdivided into 27 morphological types using the Golgi method (Mariani, 1990; Kolb et al., 1992). However, with the exception of a few well-studied types, it is still uncertain how these amacrine cells contribute to vision. We have approached this problem by identifying a marker for one common type of primate amacrine cell and using this with other known markers in multiple immunolabeling experiments to identify its neurotransmitter and to describe its contacts. We also recorded the light responses of one of these amacrine cells to full-field stimuli using intracellular electrodes and then injected the tracer Neurobiotin.

Previously, we found that amacrine cells with high levels of immunoreactive parvalbumin (PV++) made contacts with OFF starburst amacrine cells and were among those contacting OFF parasol ganglion cells in macaque retina (Bordt et al., 2006). Here, we identified these cells morphologically as one of the “knotty” amacrine cells first described by Polyak (1941) using the Golgi method and later called “stratified diffuse” by Boycott and Dowling (1969). Specifically, they were the “knotty type 2” amacrine cells first described in the macaque retina (Mariani, 1990) or, possibly, homologues of the A3 and A4 amacrine cells described in human retinas (Kolb et al., 1992). We confirmed that the PV++ amacrine cells contained immunoreactive glycine transporter-1 (Glyt-1; Pow & Hendrickson, 1999) but not immunoreactive γ-aminobutyric acid (GABA), findings suggesting that they use glycine as their neurotransmitter. We saw contacts from PV++ amacrine cells onto lobular dendrites of AII amacrine cells. Based on an earlier ultrastructural study of macaque retina (Wässle et al., 1995), we inferred that the PV++ cells are presynaptic there and inhibit the transmission of signals from the primary rod pathway. PV++ amacrine cells also contacted OFF midget bipolar cells, a finding suggesting that they receive cone input and contribute to the neural circuit that mediates high acuity vision and red–green color opponency (Kolb & Marshak, 2003). Despite the fact that most of its dendrites were in the distal half of the IPL and made contacts with axons of OFF bipolar cells, one of these cells had ON responses to full-field stimuli.

Materials and methods

Eyes from 14 macaques (6 *Macaca mulatta* and 8 *Macaca fascicularis*) were used. Some eyes were purchased from Covance Research Products (Alice, TX) or Charles River BRF (Houston, TX), and the rest were donated by other investigators. These animals were euthanized in accordance with protocols approved by the Institutional Animal Care and Use Committee prior to enucleation. The eyes were hemisected and the vitreous humor was removed with fine forceps. The posterior halves were fixed in 4% paraformaldehyde in 0.1 M phosphate buffer (pH 7.4). Fixation times varied from 1 to 4 h at room temperature or overnight at 4°C. Retinas were isolated from the retinal pigment epithelium and cut into pieces approximately 7-mm square. The pieces were either analyzed as flat mounts or sectioned vertically at 70–100 μm using a vibrating blade microtome (Leica VT1000 S; Leica Microsystems, Bannockburn, IL). No obvious species differences were noted, and both are described together here.

The tissue was double or triple labeled using antibodies to parvalbumin and one or two other primary antibodies raised in different species (Table 1). The mixtures of primary antibodies contained 0.3% Triton-X 100 and 1% normal donkey serum in phosphate-buffered saline (PBS; Sigma Aldrich, St. Louis, MO) with sodium azide, and the incubation time was 10 days at 4°C. After being rinsed several times with PBS, the tissue was incubated in either 1:200 fluorophore-conjugated or 1:1000 biotin-conjugated affinity-purified secondary antibodies made in donkeys and directed against the host species of the primary antibodies with or without 0.3% Triton-X 100 at 4°C for 1–2 days. The fluorophores used in these experiments were AlexaFluor 488 (Molecular Probes, Eugene, OR), indocarbocyanine (Cy3;

Jackson Immunoresearch, West Grove, PA), and indodicarbocyanine (Cy5; Jackson Immunoresearch). When using the avidin–biotin method, the tissue was incubated with 1:200 streptavidin-conjugated Cy3 (Jackson Immunoresearch) at 4°C for 2 days following a second set of PBS rinses. After a third series of rinses, the sections were mounted on glass slides in Vectashield mounting medium containing 4,6-diamino-2-phenylindole dihydrochloride (DAPI; H1200; Vector Laboratories, Burlingame, CA).

Images were acquired using a Zeiss 510 Meta LSM or a 510 LSM confocal microscope (Carl Zeiss, Thornwood, NY) equipped with either helium/neon and krypton/argon or helium/neon and argon lasers using a ×40 or ×63 oil immersion lens. The images were 1024 × 1024 or 2048 × 2048 pixels, and the *Z*-interval for all images was 0.5 μm. Excitation wavelengths for the individual fluorochromes were 488 nm for Alexa 488, 543 nm for Cy3, and 653 nm for Cy5. Confocal images were analyzed using LSM Image Browser (Carl Zeiss) and optimized for publication using Adobe Photoshop 6.0.1 (Adobe Systems Inc., San Jose, CA). All measurements were taken using tools available in the LSM Image Browser software package.

A piece of an eyecup from one macaque midperipheral retina was dark adapted and handled under infrared illumination using Nitemare image converters (BE Meyers, Redmond, WA). The retina was isolated from the retinal pigment epithelium, placed over a hole in a piece of filter (HAO, pore size, 0.45 μm; Millipore, Bedford, MA), and secured in a superfusion chamber with photoreceptor side upward. The preparation was superfused with Ames medium saturated with 95% O_2/5% CO_2 at a flow rate of 5 ml/min at 37°C. To position the electrodes, the preparation was viewed with a Zeiss upright fixed-stage microscope with an infrared filter over the condenser and a ×32 objective lens modified for the Hoffman modulation contrast optics (Hoffman Modulation Optics, Greenvale, NY).

The intracellular recording was then made in complete darkness using micropipettes drawn with a modified Livingston puller with omega dot tubing (1.0 mm outer diameter and 0.5 mm inner diameter). When filled with 2 M potassium acetate and measured in Ames medium, the micropipettes had tip resistances of 100–600MΩ. Microelectrode tips were filled with 3% Neurobiotin (Vector Laboratories) in 50 mM Tris and backfilled with 3 M lithium chloride. Signals were recorded with a microelectrode amplifier (Nihon Kohden, Foothill Ranch, CA). The impalement was facilitated by adjusting the negative capacitance in the electrode headstage. Voltage traces were monitored with an oscilloscope (model 5500A; Tektronix, Beaverton, OR) and then digitized, stored, and analyzed with a computer A–D system (p-clamp 8; Axon Instruments, Foster City, CA).

The preparation was stimulated with a photostimulator with a quartz halogen source (Shanghai Institute of Optical Instruments, Shanghai, China) whose intensity and wavelength could be adjusted by neutral-density filters and interference filters. The light was projected onto the preparation by means of a computer-driven moving mirror. The intensity of the unattenuated 500-nm light source measured with a radiometric detector (United Detector Technology, Santa Monica, CA) was (log $I = 0$) 1.78×10^5 photons/μm^2/s.

After the physiological experiment, Neurobiotin was injected with positive current (5 nA, 3 Hz, 30 min). Then, the tissue was fixed with 4% paraformaldehyde for 2 h, rinsed, and labeled with streptavidin-conjugated Cy3. Cell morphology and patterns of tracer coupling were visualized using a confocal microscope (Zeiss 510). Images were acquired by using a ×40 oil immersion objective, the 543-nm excitation line of a He/Ne laser, and a 560-nm long-pass filter. The techniques were very similar to those used previously to study salamander retina (Zhang et al., 2006).

Results

The perikarya of amacrine cells containing high levels of immunoreactive parvalbumin (PV ++) were found in the most proximal row of the inner nuclear layer (INL), except in central retina, defined here as 5 mm or less from the fovea, where cell densities were higher and they occupied two proximal rows in the INL. The PV++ amacrine cells labeled with all three parvalbumin antibodies had similar morphology. The perikarya had a pyriform shape and measured approximately 8 μm on the short axis and 10 μm on the long axis. The density of the perikarya was relatively high. As described previously, AII amacrine cells contained high levels of immunoreactive calretinin (Wässle et al., 1995; Mills & Massey, 1999), and immunoreactive parvalbumin and calretinin were colocalized in the perikarya of a third population of amacrine cells (Kolb et al., 2002). These CR+/PV+ amacrine cells were distinguishable from the PV++ amacrine cells by their lower levels of immunoreactive parvalbumin and the absence of dendritic labeling in the IPL (Fig. 1). Unlike the PV+/CR+ cells, the PV++ amacrine cells also contained low levels of immunoreactive calbindin (not illustrated). To compare the densities of PV++ and AII amacrine cells, 12 images from flat mounts of four different midperipheral macaque retinas, approximately 5–10 mm from the fovea, were analyzed. The average number of AII amacrine cells was 1384/mm^2 ± 422 S.D., and the average number of PV++ amacrine cells was 734/mm^2 ± 391 S.D. Thus, the density of PV++ cells was approximately half that of the AII cells. The PV++ perikarya were regularly arranged, for the most part, but there was a tendency toward clumping. In the area illustrated in Fig. 1, for example, there were 61 PV++ perikarya, of which 8 (4 pairs) were adjacent.

A single primary dendrite extended from the PV++ cell body into the IPL (Fig. 2). This dendrite was thin, measuring 0.75 ± 0.02 μm S.D (n = 10) in diameter and easily distinguished from the thicker AII amacrine cell primary dendrites. The higher order PV++ dendrites were very thin, much less than 0.5 μm in diameter, and wavy. These dendrites had many large, roughly spherical varicosities ranging from 0.5 to 2.5 μm in diameter (mean = 1.41 ± 0.47 s.d., n = 200). The largest of these varicosities was typically found at branch points in the dendrites. The varicosities were often indented in their centers; these were presumed to be sites of contacts with other cells.

Antibodies directed against choline acetyltransferase (ChAT) labeled the dendrites of starburst amacrine cells in stratum (S) 4 of the IPL, which were used as depth markers. Although these starburst cell dendrites contained immunoreactive parvalbumin, they were clearly distinguishable from the dendrites of PV++ amacrine cells by their morphology, stratification pattern, and their lower labeling intensity. Typically, the varicosities of PV++ amacrine cells extended as far as S4, as defined by the starburst cell dendrites, but not deeper into the IPL. To quantify the stratification depth of the dendrites, we measured the positions of 200 PV++ varicosities using vertical sections from the midperipheral retinas of five macaques (Fig. 3). The values were normalized by expressing the depth as a percentage of the distance from the INL to the ganglion cell layer (GCL), which were identified by the presence of DAPI-labeled perikarya (not illustrated). The varicosities of PV++ cells were typically found between 15 and 55% and had their peak density in S2, between 25 and 30% of the distance between the INL and the GCL. Of the 120 individual varicosities measured, only 14 were found at 60% or more of the distance to the GCL, and none was found at more than 85% of this distance.

The PV++ amacrine cells were not labeled with antibodies to GABA, a finding suggesting that they use the other major amacrine cell neurotransmitter, glycine. Fig. 4 shows that PV+ + cells also contained immunoreactive Glyt-1, a specific marker for glycinergic amacrine cells (Pow & Hendrickson, 1999). Both Glyt-1 and parvalbumin were found in the perikarya and throughout the dendritic arbors. Because the plexuses of processes labeled by the

antibodies to GABA and Glyt-1 were so dense, it was impossible to determine whether or not the PV++ amacrine cells made any contacts with GABAergic or other glycinergic cells. Antibodies directed against two other amacrine cell markers, the cholecystokinin precursor G6-gly and tyrosine hydroxylase, did not label the PV++ amacrine cells, and there were apparently no interactions between the populations of labeled cells.

The PV++ varicosities made frequent contacts with lobular dendrites of AII amacrine cells in S2 of the IPL (Fig. 5). Some contacts were simple appositions of the two dendrites, but in others, AII amacrine cell dendrites wrapped around the varicosities or thin dendrites of the PV++ amacrine cells, sometimes enveloping the PV++ dendrites completely. Yellow pixels were seen at the points of contact between the PV++ (green) and the CR-IR (red) processes. As a control, the AlexaFluor 488 (parvalbumin, green) image channel was rotated 180 deg around the *z*-axis relative to the Cy3 (calretinin, red) channel using Adobe Photoshop, and the numbers of yellow pixels were compared before and after the rotation. This analysis was done using seven 2048 × 2048 images from flat mounts of midperipheral retina prepared from two different macaques. A paired *t*-test indicated that the density of yellow pixels observed in the original image was significantly different ($P = 0.010$) from the inverted image. Taken with the specialized appearance of some of the contacts, this finding suggests that they were not likely to be due to chance.

PV++ amacrine cells also contacted axon terminals of OFF midget bipolar cells (Fig. 6). Recoverin-immunoreactive (RV-IR) OFF midget bipolar cell axon terminals interacted extensively with the PV++ amacrine cell dendrites. The RV-IR bipolar cell axons often traversed the INL very close to the PV++ amacrine cell primary dendrites. Sometimes, the two were intertwined as they coursed through S1 of the IPL. The contacts were mainly in S2 of the IPL, but some were also observed in S3, where the “axonal tails” of OFF bipolar cells ramified. RV-IR axon terminals were partially or completely surrounded by the larger PV++ varicosities, and smaller PV++ amacrine cell varicosities were surrounded by the OFF midget bipolar cell axon terminals. Smaller OFF bipolar axon terminals also invaginated the PV++ varicosities. Controls were done using seven 2048 × 2048 images from two different retinas and methods similar to those described above, except that the 180 deg rotation of the green image was about the *y*-axis. A significant difference in yellow pixel density ($P = 0.013$) indicated that the interactions between the PV++ amacrine cell dendrites and the RV-IR OFF midget bipolar cell axons were not likely to be due to chance. Contacts were also observed between the PV++ amacrine cell dendrites and the axon terminals of calbindin-immunoreactive, type DB3 diffuse bipolar cells, but the frequency of these contacts was low relative to that of contacts with other types of bipolar cells.

A single macaque amacrine cell from midperipheral retina, being the only one we were able to inject and record in the present study, had the knotty type 2 morphology and ON responses to full-field stimuli. The voltage responses of this amacrine cell to 500-ms steps of 500-nm light are illustrated in Fig. 7a. The cell depolarized, reaching a peak approximately 150 ms after the stimulus onset. The response then declined, but the cell remained depolarized while the stimulus was on. At higher intensities, the responses apparently saturated in amplitude, but the peaks were somewhat longer. At the highest intensity tested, there was a prolonged depolarization following the offset of the stimulus. This resembled the “rod aftereffect” first described in cat horizontal cells (Steinberg, 1969), a finding suggesting that the knotty type 2 cells receive rod input.

Based on diffusion of Neurobiotin, the injected amacrine cell appeared to be homologously coupled; 123 neighboring cells with the same morphology were labeled (Fig. 7b). That is, the perikarya, primary dendrites, and varicosities were all very similar to one another (Fig. 7c). The density of the perikarya was 1268/mm^2, a value within the range observed for PV+

+ cells at this eccentricity. The arrangement of the perikarya was not entirely regular; 24 cells (12 pairs) of the 124 in the sample had perikarya that were adjacent. Like the PV++ cells, the cells labeled with Neurobiotin all had similar indentations in the dendritic varicosities, and their dendritic stratification patterns were also the same and very similar to those of the PV++ cells (Fig. 7d). The dendritic field diameter for knotty type 2 amacrine cells at this eccentricity is not known, but using the range of diameters reported by Mariani (1990) and the density measured from Fig. 7b, the calculated dendritic overlap for the injected cells was at least 1 and may be as high as 2.

Discussion

The amacrine cells containing high levels of immunoreactive parvalbumin (PV++) have been seen in primate retinas previously. These cells were first observed in macaques and humans (Endo et al., 1986), and their neurotransmitter was later identified as glycine in macaques (Martin & Grünert, 1992; Grünert & Wässle, 1996). They were also described briefly in another study of macaque retinas, but the focus there was on a second population of diffuse amacrine cells that contained lower levels of immunoreactive parvalbumin and also immunoreactive calretinin (Kolb et al., 2002). We described contacts between PV++ amacrine cells and dendrites of OFF parasol cells filled with Lucifer yellow in S2 of macaque retinas. We also saw contacts between the PV++ amacrine cells and the dendrites of starburst amacrine cells labeled with antibodies to ChAT there (Bordt et al., 2006). Most recently, PV++ amacrine cells that contain immunoreactive glycine, but not immunoreactive GABA, were described in developing macaque retinas (Hendrickson et al., 2007). PV++ amacrine cells have also been found in baboon retinas (Sanna et al., 1993). These amacrine cells are not found exclusively in Old World monkeys; PV++ amacrine cells have been described in each of the other major groups of primates, as well. However, it was not possible to characterize the PV++ amacrine cells further in that study, and presumably in the other previous studies, because of difficulties in resolving their dendrites (Chiquet et al., 2005). Our study is the first to identify these PV++ amacrine cells morphologically.

In a number of respects, the PV++ amacrine cells resembled knotty type 2 cells described previously using the Golgi method (Mariani, 1990). Like knotty type 2 amacrine cells, the perikarya of PV++ cells in our sample were virtually all in the INL, and both types of perikarya were similar in size, approximately 8 μm in diameter. Both types of amacrine cells had relatively large varicosities; they were 1–2 μm in diameter in knotty type 2 cells and averaged 1.4 μm in diameter in PV++ cells; the other parts of the dendrites of both types were very thin. The relatively broad dendritic stratification patterns of the two types were also very similar. Dendrites of knotty type 2 amacrine cells extended from S2 to S4 of the IPL or approximately 20–80% of the distance between the INL and the GCL. The varicosities of PV++ amacrine cells were typically found between 15 and 55%, but some extended as far as 80–85%. Another result in our study was that the mean density of PV++ amacrine cells in midperipheral retina was 734/mm^2, a value that is approximately one half that of AII amacrine cells measured in our sample and described previously in macaque retina (Mills & Massey, 1999). Although the Golgi method is not quantitative, the finding that knotty type 2 cells were frequently labeled suggests that their density is also relatively high (Mariani, 1990).

Knotty type 2 amacrine cells have two homologues in humans, the A3 cells and the A4 cells. The primary difference between the A3 cells and the A4 cells is that the dendrites of A4 cells extend into S4, and the dendrites of A3 cells do not (Kolb et al., 1992). It is possible that there are also two morphological types of amacrine cells in macaques that contained high levels of immunoreactive parvalbumin, one homologous to A3 and the other to A4. The finding that a few PV++ dendritic varicosities were located between 60 and 85% and of the

distance between the INL and the GCL is consistent with this hypothesis. The spatial distribution of the PV++ perikarya also supports this hypothesis. The perikarya were sometimes adjacent to one another, but a single type of amacrine cell would be expected to have a more regular spatial distribution. On the other hand, a tendency of amacrine cell perikarya to be clumped may simply be characteristic of knotty type 2 cells. This phenomenon has also been described in a well-characterized population of amacrine cells, the displaced starburst amacrine cells in humans (Rodieck & Marshak, 1992). The perikarya of tracer-coupled cells were sometimes also adjacent, but there were no apparent morphological differences between the juxtaposed cells. If there were, indeed, both A3-like and A4-like amacrine cells, this observation could be explained by heterologous coupling between the two types. This has never been reported in glycinergic amacrine cells, but it would not be unprecedented. GABAergic amacrine cells are coupled to other morphological types of amacrine cells (Li et al., 2002; Vaney, 2004). Additional intracellular labeling experiments using a tracer such as Lucifer yellow that does not permeate gap junctions of narrow-field amacrine cells would be required to resolve this issue.

Another finding was that PV++ amacrine cells contained immunoreactive glycine transporter (Glyt-1) but not immunoreactive GABA, and therefore, they use glycine as their neurotransmitter. Glyt-1 is a more reliable marker for glycinergic neurons than glycine, itself, because it is found only in amacrine cell, not in bipolar cells that accumulate glycine *via* gap junctions with AII amacrine cells (Pow & Hendrickson, 1999). The PV++ amacrine cells resembled glycinergic amacrine cells described previously in primate retinas. That is, they were relatively common, and their perikarya were small, rarely displaced to the GCL (Koontz et al., 1993; Kalloniatis et al., 1996). The synaptic connections of glycinergic neurons have been studied previously in primate retinas using electron microscopic (EM) autoradiography with ^{3}H glycine (Frederick et al., 1984; Marc & Liu, 1985) and using EM immunohistochemistry with antibodies to glycine (Hendrickson et al., 1988). In the latter two studies, the heavily labeled Gly2 amacrine cells were identified as AII amacrine cells based on their morphology and spatial density, and the rest were classified as Gly1. Based on our findings that the PV++ amacrine cell processes did not contain immunoreactive calretinin and were morphologically different from AII cells in many ways, we concluded that they are a subset of the Gly1 cells. Because Gly1 cells are heterogeneous, it was not possible to directly compare our results with those from the EM studies. However, some features of the glycinergic synapses described there were helpful to us in interpreting the images from confocal microscopy. For example, the synapses were often found at sites where the presynaptic cells were indented by the postsynaptic cell or *vice versa*.

A major finding was that PV++ amacrine cells made extensive contacts with OFF midget bipolar cell axon terminals. These were identified using antibodies to recoverin, a specific marker for these cells in Old World monkeys (Milam et al., 1993; Wässle et al., 1994; Jacoby et al., 2000; Jusuf et al., 2006). It was not possible to predict the polarity of the interactions between PV++ amacrine cells and OFF midget bipolar cells with certainty, but in central macaque retina, amacrine cells receive synapses from all the bipolar cell axons that impinge on their dendrites (Calkins & Sterling, 1996). It is also possible that the amacrine cells were exclusively presynaptic or else both pre- and postsynaptic there; 77% of the amacrine cells that receive input from midget bipolar cells also make reciprocal synapses (Calkins & Sterling, 1996). These findings suggest that the PV++ amacrine cells contribute to the neural circuit providing input to OFF midget ganglion cells, the cells mediating high acuity vision and red–green color vision (reviewed by Kolb & Marshak, 2003).

PV++ amacrine cells also contacted lobular dendrites of calretinin-immunoreactive AII amacrine cells in S2 (Wässle et al., 1995; Mills & Massey, 1999). Under the conditions used in our study, dendrites of the AII cells were the only structures in the IPL containing

immunoreactive calretinin. Although perikarya containing both immunoreactive calretinin and immunoreactive parvalbumin were labeled as described previously (Kolb et al., 2002), the dendrites of these amacrine cells were unlabeled in our material. Because lobular AII dendrites receive synapses from amacrine cells in S2 but do not make any synapses onto amacrine cells there (Wässle et al., 1995), we concluded that the PV++ amacrine cells were presynaptic at these contacts. Based on previous results in rat retinas, glycine would be expected to inhibit the AII cells (Boos et al., 1993). This finding suggests that another function of PV++ amacrine cells is to inhibit transmission of information from rods *via* rod bipolar cells and AII amacrine cells, the most sensitive of the known rod pathways (Bloomfield & Dacheux, 2001).

Most of the dendrites of PV++ amacrine cells were found in the distal half of the IPL, and they made contacts with OFF bipolar cells. However, a cell with the same morphology had ON responses to full-field light stimuli, presumably mediated by inputs from unidentified ON bipolar cells in the proximal half of the IPL (Dacey et al., 2000). In this respect, they resembled AII amacrine cells, which receive inputs from OFF bipolar cells in primates (Wässle et al., 1995) but, nevertheless, have ON responses to light (Dacey, 1999). Like primate AII cells, PV++ amacrine cells were also well coupled under dark-adapted conditions (Mills & Massey, 1995). Taken together, these findings suggest that one function of PV++ amacrine cells is inhibition of the OFF pathway. Three previous studies provide evidence for this inhibition of OFF cells by ON amacrine cells in primates. After intravitreal injections of L-2-amino-4-phosphonobutyrate (APB), OFF cells in the macaque lateral geniculate nucleus show transient increases in both maintained activity and light responses (Schiller, 1984). The same effect of APB was observed in a subset of macaque OFF retinal ganglion cells *in vitro* (Cohen & Miller, 1994). More recently, APB was shown to increase the light responses of OFF parasol ganglion cells in macaque retinas (Field et al., 2007). Similar effects, known as “vertical inhibition” or “crossover inhibition,” have been observed in retinas of other species, as well (reviewed by Manookin et al., 2008).

In summary, we propose that parvalbumin is a marker for one of the most common types of amacrine cells in the primate retina, the knotty type 2 cells. These are narrow-field glycinergic amacrine cells, and under dark-adapted conditions, they are extensively coupled to other amacrine cells of the same type and have ON responses to light. One possible function for knotty type 2 cells is inhibition of the OFF pathway at the onset of increments in light intensity. They also make contacts onto the lobular dendrites of AII amacrine cells. Based on previous ultrastructural studies, these are likely sites of synapses that would inhibit the transmission of rod signals to the OFF pathway.

Acknowledgments

We thank Drs. Allan Wiechmann, David Pow, and John DelValle for the gift of antibodies used in this study; Drs. Jocelyne Bachevalier and Daniel Felleman for donating retinal tissue used in these experiments; Dr. Alice Chuang for her help with statistical analysis; and Ms. Andrea Bordt and Ms. Maria Bernal for their excellent technical assistance. This work was supported by the Retina Research Foundation, Research to Prevent Blindness, and National Eye Institute grants EY06472, EY10608, EY 04446, and EY02520.

References

Bloomfield SA, Dacheux R. Rod vision: Pathways and processing in the mammalian retina. Progress in Retina and Eye Research. 2001; 20:351–384.

Boos R, Schneider H, Wässle H. Voltage- and transmitter-gated currents of AII-amacrine cells in a slice preparation of the rat retina. The Journal of Neuroscience. 1993; 13:2874–2888. [PubMed: 7687279]

Bordt AS, Hoshi H, Yamada ES, Perryman-Stout WC, Marshak DW. Synaptic input to OFF parasol ganglion cells in macaque retina. The Journal of Comparative Neurology. 2006; 498:46–57. [PubMed: 16856174]

Boycott BB, Dowling JE. Organization of the primate retina: Light microscopy. Philosophical Transactions of the Royal Society of London. 1969; 799:109–184.

Calkins DJ, Sterling P. Absence of spectrally specific lateral inputs to midget ganglion cells in primate retina. Nature. 1996; 381:613–615. [PubMed: 8637598]

Chiquet C, Dkhissi-Benyahya O, Cooper HM. Calcium-binding protein distribution in the retina of strepsirhine and haplorhine primates. Brain Research Bulletin. 2005; 68:185–194. [PubMed: 16325019]

Cohen ED, Miller RF. The role of NMDA and non-NMDA excitatory amino acid receptors in the functional organization of primate retinal ganglion cells. Visual Neuroscience. 1994; 11:317–332. [PubMed: 8003456]

Dacey D, Packer OS, Diller L, Brainard D, Peterson B, Lee B. Center surround receptive field structure of cone bipolar cells in primate retina. Vision Research. 2000; 40:1801–1811. [PubMed: 10837827]

Dacey DM. Primate retina: Cell types, circuits, and color opponency. Progress in Retinal and Eye Research. 1999; 18:737–763. [PubMed: 10530750]

Dowling JE, Boycott BB. Organization of the primate retina: Electron microscopy. Proceedings of the Royal Society B: Biological Sciences. 1966; 166:80–111.

Endo T, Kobayashi M, Kobayashi S, Onaya T. Immunocytochemical and biochemical localization of parvalbumin in the retina. Cell and Tissue Research. 1986; 234:213–217. [PubMed: 3943121]

Field GD, Sher A, Gauthier JL, Greschner M, Shlens J, Litke AM, Chichilinisky EJ. Spatial properties and functional organization of small bistratified ganglion cells in primate retina. The Journal of Neuroscience. 2007; 27:13261–13272. [PubMed: 18045920]

Frederick JM, Rayborn ME, Hollyfield JG. Glycinergic neurons in the human retina. The Journal of Comparative Neurology. 1984; 227:159–172. [PubMed: 6088595]

Grünert U, Wässle H. Glycine receptors in the rod pathway of the macaque monkey retina. Visual Neuroscience. 1996; 13:101–115. [PubMed: 8730993]

Hendrickson A, Yan YH, Erickson A, Possin D, Pow D. Expression patterns of calretinin, calbindin and parvalbumin and their colocalizations in neurons during development of Macaca monkey retina. Experimental Eye Research. 2007; 85:587–601. [PubMed: 17845803]

Hendrickson AE, Koontz MA, Pourcho RG, Sarthy PV, Goebel DJ. Localization of glycine-containing neurons in the Macaca monkey retina. The Journal of Comparative Neurology. 1988; 273:473–487. [PubMed: 3209734]

Hokoc JN, Mariani AP. Tyrosine hydroxylase immunoreactivity in the rhesus monkey retina reveals synapses from bipolar cells to dopaminergic amacrine cells. The Journal of Neuroscience. 1987; 7:2785–2793. [PubMed: 2887643]

Jacoby RA, Wiechmann AF, Amara SG, Leighton BH, Marshak DW. Diffuse bipolar cells provide input to OFF parasol ganglion cells in the macaque retina. The Journal of Comparative Neurology. 2000; 416:6–18. [PubMed: 10578099]

Jusuf PR, Martin PR, Grünert U. Synaptic connectivity in the midget-parvocellular pathway of primate central retina. The Journal of Comparative Neurology. 2006; 494:260–274. [PubMed: 16320234]

Kalloniatis M, Marc RE, Murry RF. Amino acid signatures in the primate retina. The Journal of Neuroscience. 1996; 16:6807–6829. [PubMed: 8824321]

Kolb H, Linberg KA, Fisher SK. Neurons of the human retina: A Golgi study. The Journal of Comparative Neurology. 1992; 318:147–187. [PubMed: 1374766]

Kolb H, Marshak D. The midget pathways of the primate retina. Documenta Ophthalmologica. 2003; 106:67–81. [PubMed: 12675488]

Kolb H, Zhang L, Dekorver L, Cuenca N. A new look at calretinin-immunoreactive amacrine cell types in the monkey retina. The Journal of Comparative Neurology. 2002; 453:168–184. [PubMed: 12373782]

Koontz MA, Hendrickson AE. Stratified distribution of synapses in the inner plexiform layer of primate retina. The Journal of Comparative Neurology. 1987; 263:591–592.

Koontz MA, Hendrickson LE, Brace ST, Hendrickson AE. Immunocytochemical localization of GABA and glycine in amacrine and displaced amacrine cells of macaque monkey retina. Vision Research. 1993; 33:2617–2628. [PubMed: 8296457]

Li W, Zhang J, Massey SC. Coupling pattern of S1 and S2 amacrine cells in the rabbit retina. Visual Neuroscience. 2002; 19:119–131. [PubMed: 12385625]

Manookin MB, Beaudoin DL, Ernst ZR, Flagel LI, Demb JB. Disinhibition combines with excitation to extend the operating range of the OFF visual pathway in daylight. The Journal of Neuroscience. 2008; 28:4136–4150. [PubMed: 18417693]

Marc RE, Liu WL. (^{3}H) glycine-accumulating neurons of the human retina. The Journal of Comparative Neurology. 1985; 232:241–260. [PubMed: 2982926]

Mariani AP. Amacrine cells of the rhesus monkey retina. The Journal of Comparative Neurology. 1990; 301:382–400. [PubMed: 2262597]

Marshak DW, Aldrich LB, Del Valle J, Yamada T. Localization of immunoreactive cholecystokinin precursor to amacrine cells and bipolar cells of the macaque monkey retina. The Journal of Neuroscience. 1990; 10:3045–3055. [PubMed: 2398370]

Martin PR, Grünert U. Spatial density and immunoreactivity of bipolar cells in the macaque monkey retina. The Journal of Comparative Neurology. 1992; 323:269–287. [PubMed: 1401260]

Milam AH, Dacey DM, Dizhoor AM. Recoverin immunoreactivity in mammalian cone bipolar cells. Visual Neuroscience. 1993; 10:1–12. [PubMed: 8424920]

Mills SL, Massey SC. Differential properties of two gap junctional pathways made by AII amacrine cells. Nature. 1995; 377:734–737. [PubMed: 7477263]

Mills SL, Massey SC. AII amacrine cells limit scotopic acuity in central macaque retina: A confocal analysis of calretinin labeling. The Journal of Comparative Neurology. 1999; 411:19–34. [PubMed: 10404105]

Nishimura Y, Schwartz ML, Rakic P. Localization of γ-aminobutyric acid and glutamic acid decarboxylase in rhesus monkey retina. Brain Research. 1985; 359:351–355. [PubMed: 3907753]

Polyak, SL. The Retina. Chicago, IL: Chicago University Press; 1941.

Pow DV, Hendrickson AE. Distribution of the glycine transporter glyt-1 in mammalian and nonmammalian retinae. Visual Neuroscience. 1999; 16:231–239. [PubMed: 10367958]

Rodieck RW, Marshak DW. Spatial density and distribution of choline acetyltransferase immunoreactive cells in human, macaque and baboon retinas. The Journal of Comparative Neurology. 1992; 321:46–64. [PubMed: 1613139]

Sanna PP, Keyser KT, Celio MR, Karten HJ, Bloom FE. Distribution of parvalbumin immunoreactivity in the vertebrate retina. Brain Research. 1993; 600:141–150. [PubMed: 8422581]

Schiller PH. The connections of the retinal on and off pathways to the lateral geniculate nucleus of the monkey. Vision Research. 1984; 24:923–932. [PubMed: 6506480]

Steinberg RH. The rod after-effect in S-potentials from the cat retina. Vision Research. 1969; 9:1345–1355. [PubMed: 5358839]

Vaney DI. Type 1 nitrergic (ND1) cells of the rabbit retina: Comparison with other axon-bearing amacrine cells. The Journal of Comparative Neurology. 2004; 474:149–171. [PubMed: 15156584]

Wässle H, Grünert U, Chun MH, Boycott BB. The rod pathway of the macaque monkey retina: Identification of AII-amacrine cells with antibodies against calretinin. The Journal of Comparative Neurology. 1995; 361:537–551. [PubMed: 8550898]

Wässle H, Grünert U, Martin PR, Boycott BB. Immunocytochemical characterization and spatial distribution of midget bipolar cells in the macaque monkey retina. Vision Research. 1994; 34:561–579. [PubMed: 8160377]

Yamada ES, Dmitrieva N, Keyser KT, Lindstrom JM, Hersh LB, Marshak DW. Synaptic connections of starburst amacrine cells and localization of acetylcholine receptors in primate retinas. The Journal of Comparative Neurology. 2003; 461:76–90. [PubMed: 12722106]

Zhang AJ, Zhang J, Wu SM. Electrical coupling, receptive fields, and relative rod/cone inputs of horizontal cells in the tiger salamander retina. The Journal of Comparative Neurology. 2006; 499:422–431. [PubMed: 16998920]

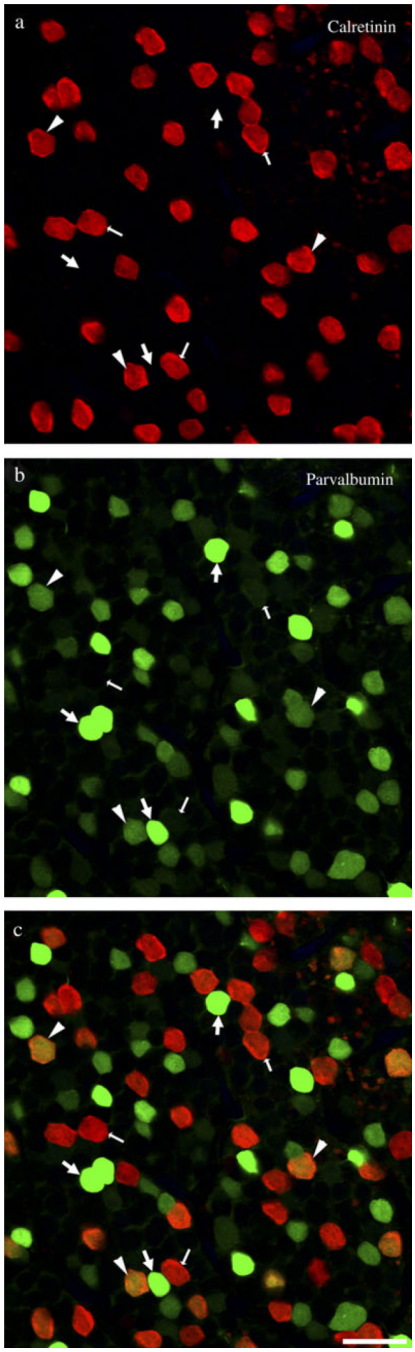

Fig. 1.

(Color online) Amacrine cell perikarya containing immunoreactive parvalbumin (green) and calretinin (red) in macaque midperipheral retina (5–10 mm from the fovea). Large arrows indicate amacrine cells containing high levels of immunoreactive parvalbumin (PV++). Small arrows indicate amacrine cells containing only immunoreactive calretinin (CR-IR). Arrowheads indicate cells containing low levels of immunoreactive parvalbumin as well as high levels of immunoreactive calretinin (CR+/PV+). (**a**) Separation of channels showing cells positive for calretinin (red). (**b**) Separation of channels showing cells positive for parvalbumin (green). (**c**) Images in (**a**) and (**b**) were merged. Cells containing high levels of

parvalbumin (PV++) do not contain calretinin. Colocalization of parvalbumin and calretinin occurs only in the perikarya of cells containing low levels of parvalbumin. Single 0.5-μm optical section. Scale bar = 20 μm.

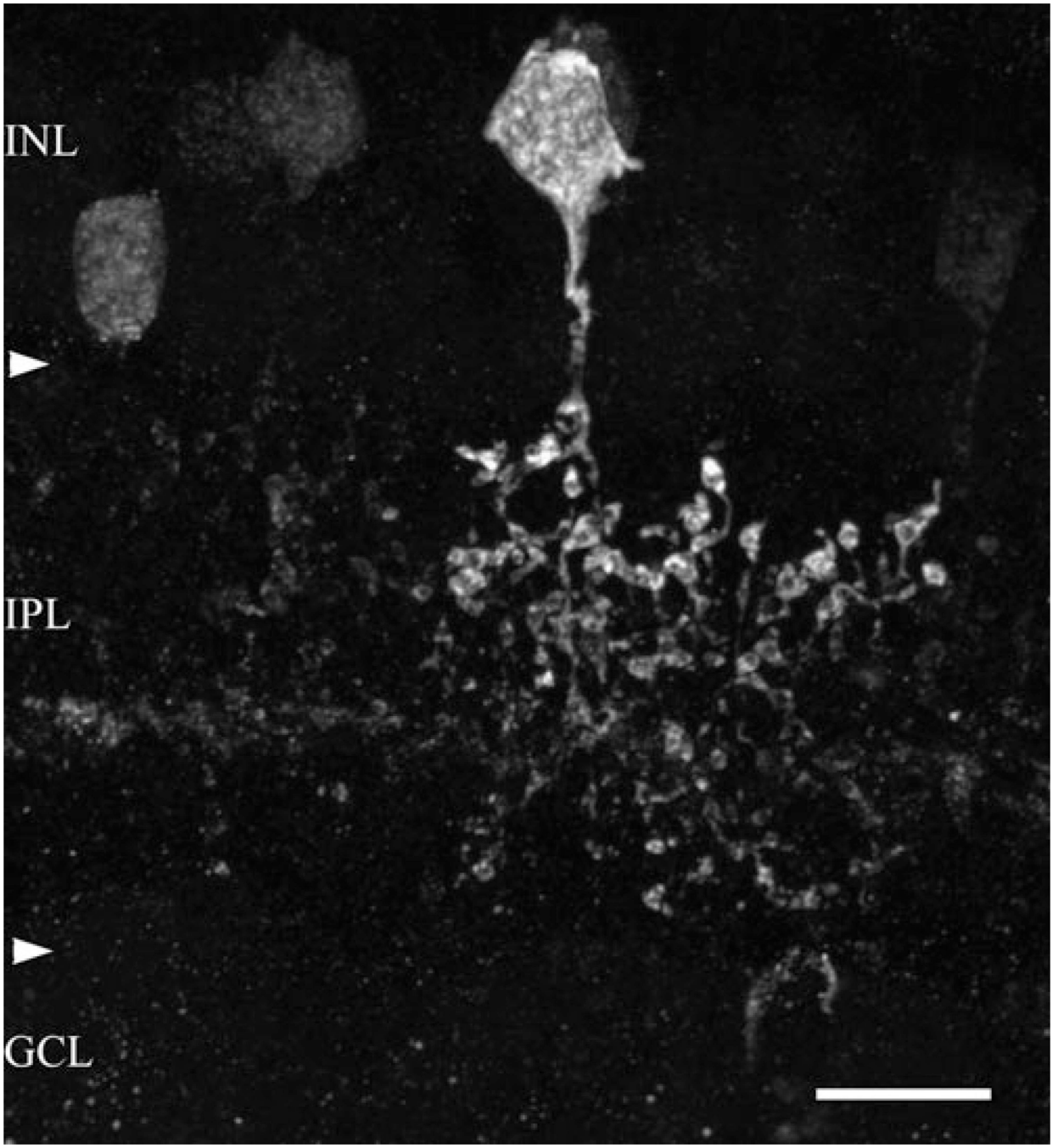

Fig. 2.

An amacrine cell containing a high level of immunoreactive parvalbumin (PV++) in a vertical section from central macaque retina (<5 mm from the fovea). A single primary dendrite extended from the perikaryon into stratum 2 (S2) of the IPL, where its thin dendrites had numerous large varicosities. Many varicosities were indented, and these were often the sites of interactions with other cell types. The horizontal band of faintly labeled processes seen in the proximal half of the IPL consists of starburst amacrine cell dendrites; this was confirmed by double-labeling experiments using an antibody directed against ChAT (not illustrated). Arrowheads demarcate the boundaries of the IPL. This image is a projection of 21 consecutive 0.5-μm optical sections. Scale bar = 10 μm.

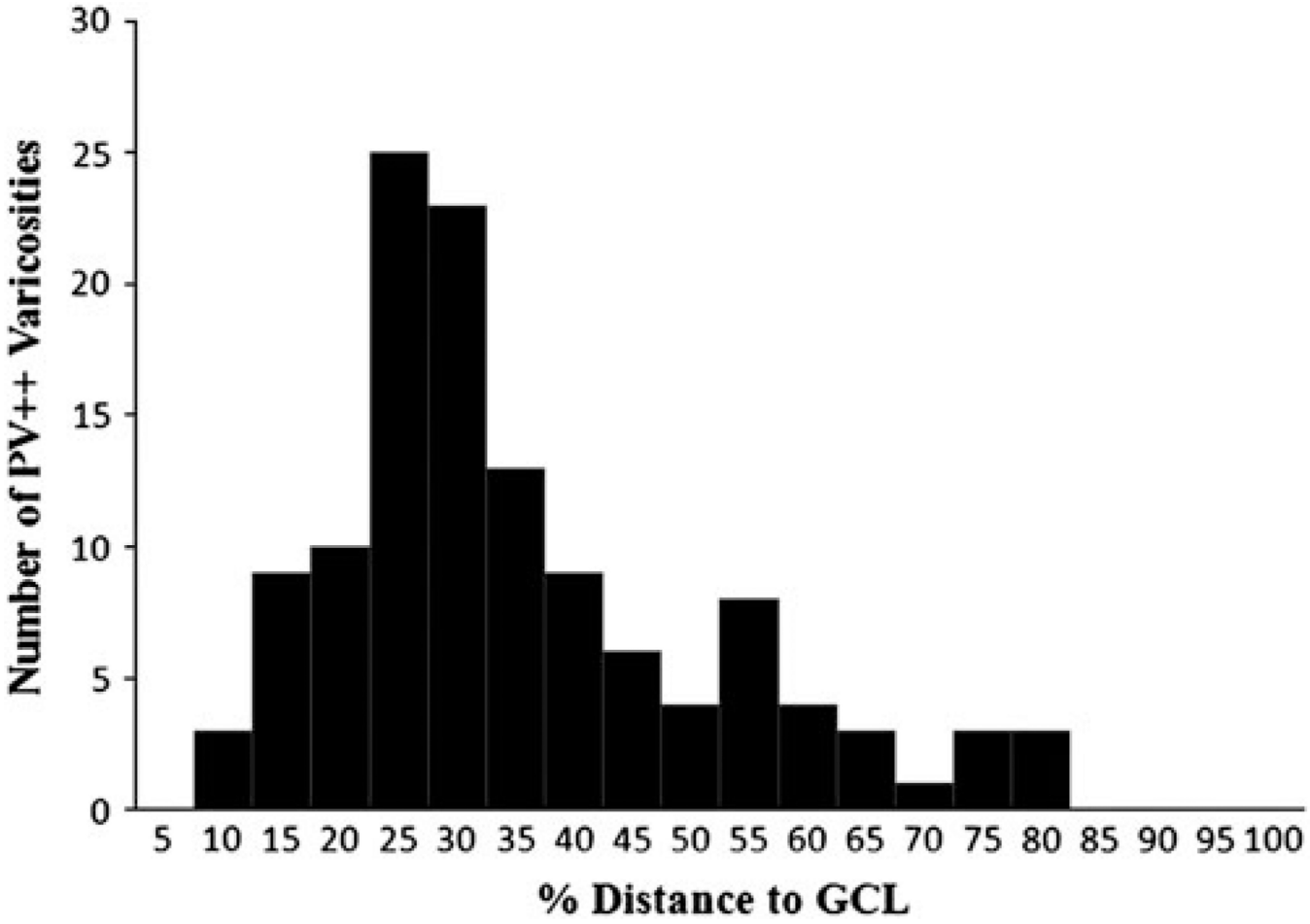

Fig. 3.

Distribution of PV++ varicosities in the IPL in midperipheral retina (5–10 mm from the fovea). Each bin represents 5% of distance from the INL to the GCL, with the first bin encompassing the distance from 0 to 5%, the second from 5 to 10%, and so on. The majority of PV++ varicosities were found between 15 and 60% of the distance to the GCL.

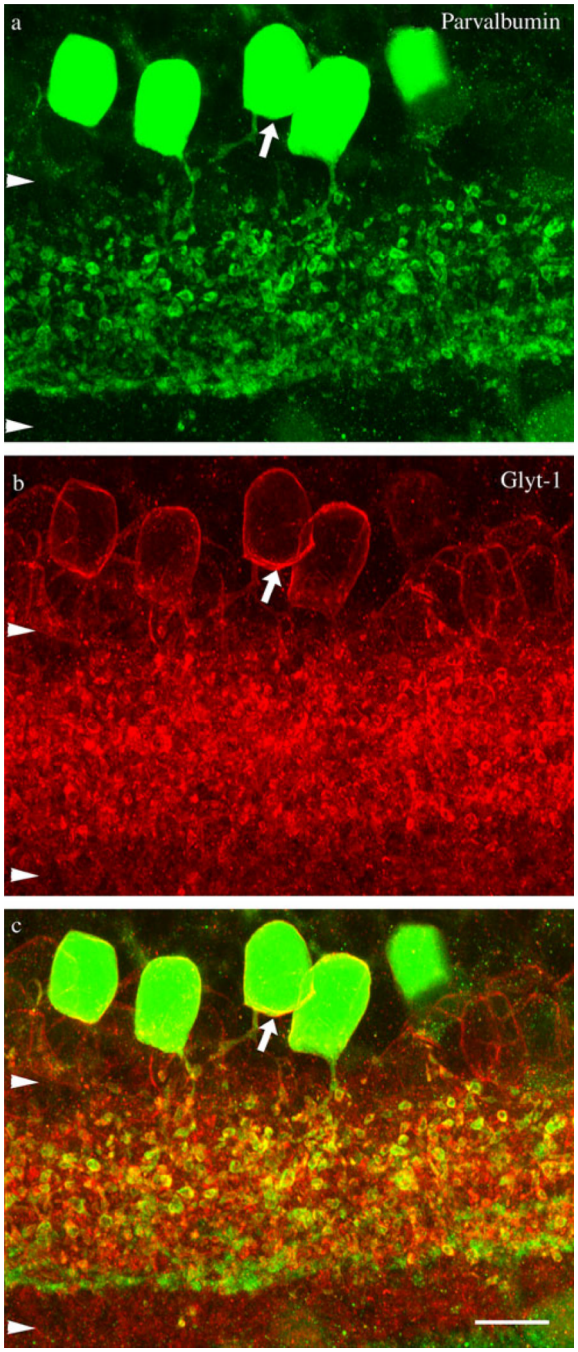

Fig. 4.

(Color online) Colocalization of immunoreactive parvalbumin and Glyt-1 in a vertical section through midperipheral retina (5–10 mm from the fovea). (**a**) Separation of channels showing PV++ amacrine cells (green). Five PV++ amacrine cells are strongly immunoreactive for parvalbumin (green). (**b**) Separation of channels showing only Glyt-1 labeling (red). Glyt-1 labels several types of glycinergic amacrine cells. The cell located at the far right is out of focus; it is labeled in the adjacent sections (not illustrated). (**c**) The two markers were colocalized (yellow). This is particularly clear in the area marked by the

arrow. Arrowheads demarcate boundaries of the IPL. This image is a projection of 27 consecutive 0.5-μm optical sections. Scale bar = 10 μm.

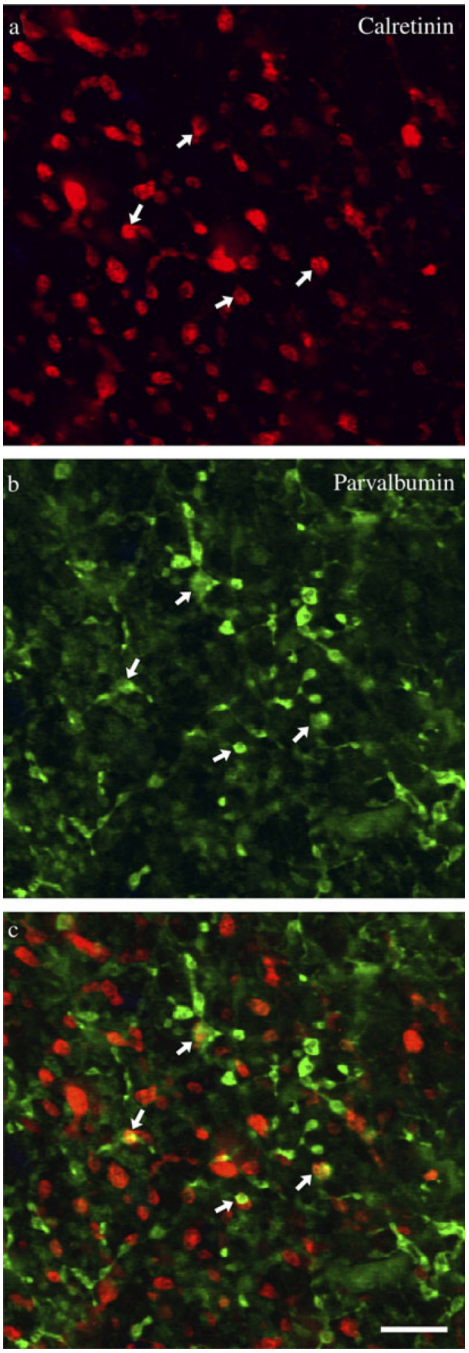

Fig. 5.

(Color online) Contacts between PV++ amacrine cells and AII amacrine cells. PV++ amacrine cells (green) contacted calretinin-immunoreactive (CR-IR) AII amacrine cells (red) in S2 of the IPL in this flat mount from midperipheral macaque retina (5–10 mm from the fovea). Images are single 0.5-μm optical sections. (**a**) Separation of channels showing only (CR-IR) AII lobular dendrites (red). (**b**) Separation of channels showing only PV++ dendrites with varicosities (green). (**c**) Arrows indicate sites of PV++ varicosity (green) and AII lobular dendrite (red) interactions (yellow). Note that AII amacrine cell lobular dendrites are large in comparison to PV++ varicosities. Scale bar = 10 μm.

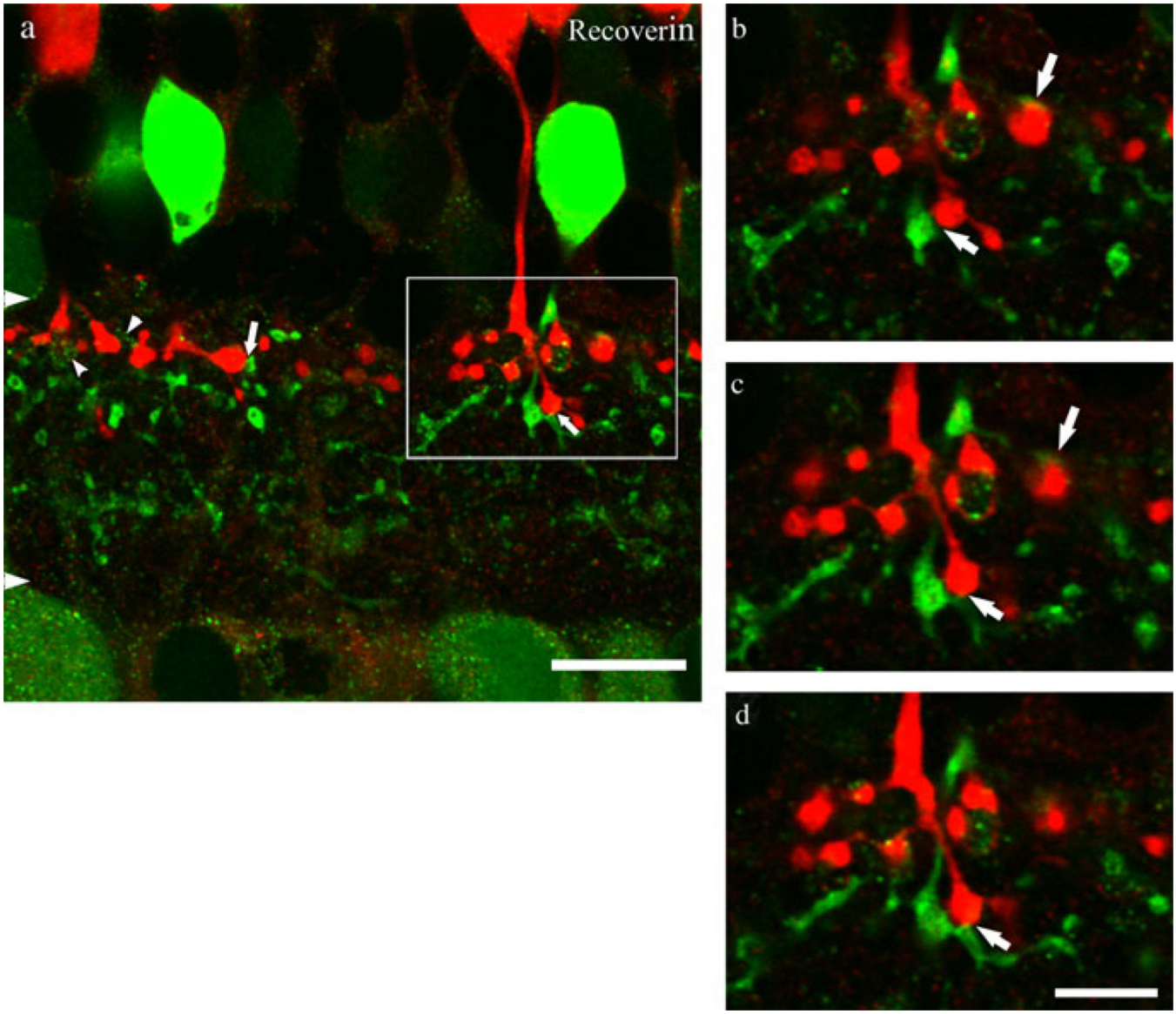

Fig. 6.

(Color online) Contacts between PV++ amacrine cells and OFF midget bipolar cells. (**a**) PV ++ amacrine cells (green) contacted RV-IR OFF midget bipolar cell axons (red). Retinal ganglion cell dendrites are also lightly labeled, but they can be distinguished from amacrine cell dendrites because the labeling is granular (small arrowheads). Arrows indicate sites of contact between PV++ and OFF midget bipolar cell axon terminals. Arrowheads demarcate boundaries of the IPL. This image is a projection of three consecutive 0.5-μm optical sections, which are shown individually as insets (**b**–**d**). Scale bar = 10 μm. (**b**–**d**) Consecutive 0.5-μm single optical sections illustrating contacts (arrows) between PV++ amacrine cells (green) and OFF midget bipolar cell axon terminals (red). Scale bar = 5 μm.

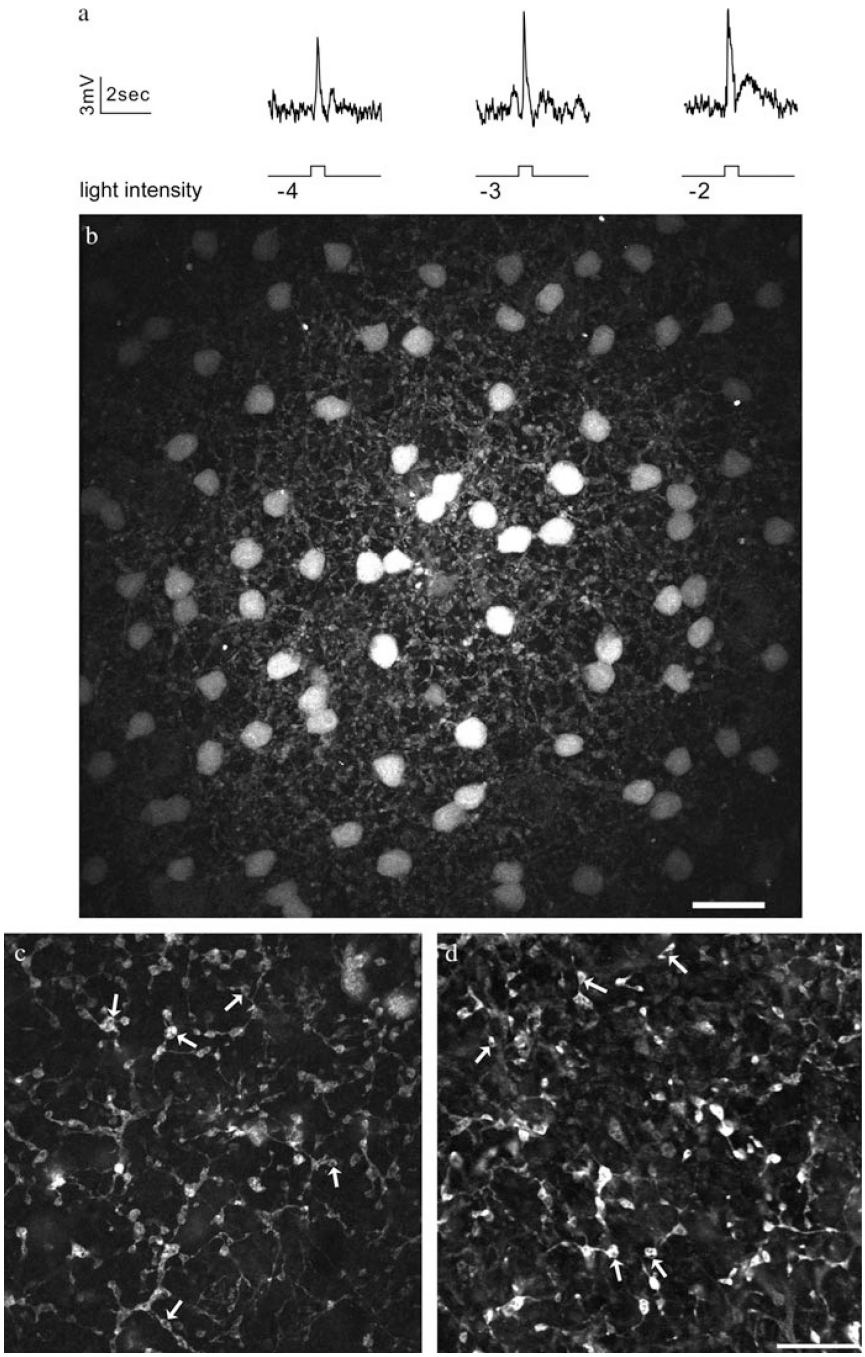

Fig. 7.

Light responses and tracer coupling of knotty type 2 amacrine cells in *Macaca fascicularis* retina. (**a**) Light responses were recorded with intracellular electrodes from a dark-adapted knotty type 2 amacrine cell. Stimuli were full field, 500 nm, and 500 ms in duration. Stimulus intensities ranged from 17.8 ($\log_{10} I = -4$) to 1.78×10^3 ($\log_{10} I = -2$) photons/μm^2/s. (**b**) Under these conditions, Neurobiotin injected into one knotty type 2 amacrine cell spread to 123 neighboring amacrine cells of the same morphological type. This image is a projection of fourteen 1-μm optical sections. Scale bar = 20 μm. (**c**) This is a single 2-μm optical section through S2 of the IPL. Neurobiotin-injected knotty type 2 amacrine cell

dendrites have numerous varicosities (arrows). (**d**) This is a single 0.5-μm optical section through S2 of the IPL. PV++ amacrine cell dendrites and varicosities in midperipheral retina (5–10 mm from the fovea) are very similar morphologically to the knotty type 2 amacrine cell dendrites. Scale bar = 10 μm.

Table 1

Antibodies used in this study

Antibody	Source, catalog number, lot number	Species raised in	Immunogen	Working dilution	References
Parvalbumin	Sigma[a], P3088, clone PARV-19	Mouse	Purified frog muscle parvalbumin	1:1000	Kolb et al. (2002)
Parvalbumin	Swant[b], McAB 235, lot 10–11 (F)	Mouse	Purified carp muscle parvalbumin	1:10,000	Kolb et al. (2002)
Parvalbumin	Swant[b], PV-28, lot 5.5	Rabbit	Rat muscle parvalbumin	1:1000, 1:2000	Kolb et al. (2002)
Calbindin	Sigma[a], C1848, D-28K	Mouse	Bovine kidney calbindin-D	1:1000	Chiquet et al. (2005)
Calbindin	Sigma[a], C8666, clone CL-300	Mouse	Chicken gut calbindin-D	1:1000	Chiquet et al. (2005)
Calretinin	Chemicon[c], Ab1559, lot 21070005	Goat	Guinea pig calretinin	1:1000	Mills and Massey (1999)
Calretinin	Chemicon[c], AB149, lot 18040705	Rabbit	Guinea pig calretinin	1:1000	Mills and Massey (1999)
ChAT	Chemicon[c], AB144P, lot 23080178	Goat	Human placental enzyme	1:200	Yamada et al. (2003)
Recoverin	Dr. Allan Wiechmann[d], 320-4	Rabbit	Human retinal recoverin	1:10,000	Milam et al. (1993)
Glyt-1	Dr. David V. Pow[e]	Guinea pig	Synthetic Glyt-1 peptide	1:1000	Pow and Hendirckson (1999)
Glyt-1	Biogenesis[f], 4710–8050, lot 21031351	Goat	K-A-Q-I-P-I-V-G-S-N-G-S-S-R-L-Q-D-S-R	1:1000	Pow and Hendirckson (1999)
G6-gly	Dr. John Del Valle[g], rabbit 6, bleed 6	Rabbit	Tyr-Gly-Trp-Met-Asp-Phe-Gly	1:1500	Marshak et al. (1990)
GABA	Chemicon[c], AB5016	Rabbit	GABA-gluteraldehyde	1:1000	Nishimura et al. (1985)
TH16	Sigma[a], T 2928, lot 021K4882	Mouse	Purified rat tyrosine hydroxylase	1:10,000	Hokoc and Mariani (1987)

[a] Sigma-Aldrich, St. Louis, MO.

[b] Swant, Bellinzona, Switzerland.

[c] Chemicon International/Millipore, Billerica, MA.

[d] Dr. Allan Wiechmann, University of Oklahoma Health Sciences Center, Oklahoma City, OK.

[e] Dr. David V. Pow, University of Newcastle, New South Wales, Australia.

[f] Biogenesis, Brentwood, NH.

[g] Dr. John Del Valle, University of Michigan, Ann Arbor, MI.